scientific reports

Check for updates

OPEN

Research on the mechanical behavior of compression molding for simulated polymer-bonded explosives

Xiaoyang Wu✉, Jun Tao✉, Bo Wang, Haichao Ren & Yiping Wang

The compression molding process of polymer bonded explosive (PBX) is a typical black-box process. It is of great significance to study the compression molding of PBX for safe production and high-quality molding. A two-dimensional mesoscopic model of polygonal crystal based on Python code is developed to analyze the mechanical behavior of granular simulated explosives compression molding. The influence of friction on the reaction force of discharge head and the crystal breakage rate is obtained through the differentiation study with different friction coefficients. It is found that when the friction coefficient is 0.3, the reaction force is 35.5% higher than that without friction, and the crystal damage rate is increased by 13.6%. By analyzing the change of crystal temperature, it can be known that the temperature of the crystal increases by 32.7℃ after compression, and it can be speculated that the hot spots are generated by the friction between the mold wall and the crystal as well as the breakage of chemical bond when the crystal is broken.

Polymer bonded explosive (PBX) is a typical representative of modern mixed explosives[1,2], which is composed of powdered energetic crystals and polymer binder. The commonly used charge molding processes include press-fitting, pouring and casting[3,4], among which press-fitting is a typical charge method. Because of its advantages of high molding density, easy to control the molding size, wide range of applications, etc., it is widely used in the preparation of weapons and ammunition of various arms such as navy, land, air and rocket army[5–7]. During the compression molding process of PBX explosives, significant density gradients tend to develop within the material, which critically affects both the detonation wave propagation accuracy and mechanical performance stability of explosive charges. Therefore, systematically investigating the spatiotemporal evolution of density distribution during molding and fundamentally revealing the formation mechanisms of density inhomogeneity are of substantial scientific significance and engineering value for enhancing energetic material performance. In recent years, a number of burning and explosion accidents have occurred in the process of explosives pressing at home and abroad, resulting in serious casualties and property losses. Various countries pay more and more attention to safety in production[8–10], so it is more and more important to study the production of polymer bonded explosives by press-loading, aiming at reducing explosion accidents and improving safety in production.

At present, the key parameters of the press-fitting process are in a "black box" state, and it is difficult to observe the experiment, and the particle flow in the pressing process is complicated and the material sensitivity is high. At this stage, the experimental test mainly focuses on the mechanical properties of the compression molding in terms of density, modulus and crystal damage. Thompson[11] studied the relationship between the density and mechanical properties of grain manufactured by isostatic pressing and molding processes, and found that the tensile and compressive strength of most samples increased with the increase of density. Herman[12] investigated the effects of binder composition, crystal particle size distribution and pressing temperature on the compressive strength and elastic modulus of the molded samples. It is found that the binder system plays a dominant role in mechanical behavior, but the particle size distribution and pressing conditions also slightly affected the elasticity and strength of the materials. Jia[13] conducted compressive shear tests on PBX simulators using the variable angle shear test method with loading angles of θ (0, 15, 30, 45, 60, 75, 90), established the Mohr-Coulomb (M-C) criterion for the power function of PBX simulators and predicted the compressive strength of PBX simulators.

When the pressing force is increased, the explosive crystal inside the grain will be damaged and fractured. Chen[14] used radiation x-ray computed tomography, scanning electron microscopy, laser particle size analyzer and other instruments to study the damage evolution and mechanism of particles under single and repeated

Xi'an Modern Chemistry Research Institute, Xi'an 710065, China. ✉email: wxyxian204@163.com; 634105233@qq.com

compression of explosive substitutes. It is found that the initial pores and cracks produced by particle crushing are the main mechanism of damage. Tan[15] found that the pressure change mainly affects the elastic twin crystal band. When the pressure increases, the twin crystal deformation is restrained and fractured due to the influence of crystal defects. The greater the pressure, the more severe the fracture is. The fracture crack occurs mainly along the interface between the binder and the particle crystal, and a small part propagates along the particle crystal and the interior of the binder. The indirect contact of the particles and the twin crystal surface are prone to stress concentration.

In recent years, with the continuous development of the finite element method, some researchers began to study the compression process of PBX by combining simulation with experiment or simulation, aiming to make the black-box process transparent. Zhang[16] studied the initial Poisson's ratio of PBX explosives and the mechanical properties under quasi-static compression. At the same time, the simulation results verified that PBX crystals mainly suffered transgranular fracture under quasi-static compression. Hagengruber[17] observed the crystal morphology of PBX explosives before and after compression based on scanning electron microscope (SEM), and analyzed the micro-fracture and elastic-plastic deformation of solid grains by finite-discrete element method (FDEM). Tang[18] built a two-dimensional microscopic model with circular random distribution, and focused on the internal stress, temperature change and particle deformation during extrusion process. Through the analysis results, it was found that multiple stress chains were formed between the particles and the contact surface, which propagated downward along the contact surface. From the temperature analysis, it can be seen that the compression molding temperature is up to 20℃.

Sun[19,20] developed a new two-scale discrete element method (DEM) model to study the compression molding of PBX composite powders, which elucidated the characteristics of the pore distribution and the density evolution law at multiple stages during the compression densification process. The potential causes of density inhomogeneity and stress attenuation are explained from the perspective of energy dissipation for the first time. Xiao[21] designed a finite element model based on the real crystal morphology, and used the cohesive model (CZM) to characterize the damages. It was found that the damage mode changed with the change of strain rate, and exhibited the nonlinear stress-strain on microscopic scale. Guo[22] based on experiments and DEM simulation, studied the mechanical properties and microscopic mechanical behavior of cyclotetramethylene tetranitramine (HMX) polymer bonded explosives with different crystal sizes during the molding process. It was found that the large-sized crystals were more broken under the same pressure, and the density of the molded grain was higher, but the strength was weaker than that of the small-sized grains. Pan[23] analyzed the stress distribution of PBX composites by finite element method, and established the mathematical model among ultrasonic attenuation coefficient, particle volume fraction and ultrasonic frequency. As a typical heterogeneous composite material, the density evolution of PBX is highly sensitive to the morphological characteristics and packing structures of irregular explosive crystals, as well as their high powder-loading features. However, current studies predominantly employ oversimplified virtual tetrahedrons as crystal templates, which fail to accurately represent the complex geometries and multiscale packing behaviors of real explosive crystals (e.g., HMX, RDX)[24,25]. This limitation constitutes a critical technical challenge in PBX geometric modeling.Furthermore, the compression molding of PBX is inherently a complex multiphysics process involving coordinated evolution of particle assemblies. Precise simulation requires not only mesoscale modeling of crystal microstructures but also macroscale representation of sufficient composite powder particles. Although existing strategies using particle clusters can effectively capture crystal fracture behavior at mesoscale, their computational inefficiency severely restricts the simulated system size at macroscale, thereby hindering accurate prediction of regional density gradients during compaction.Thus, the key scientific challenge lies in synergistically achieving: (1) high-fidelity geometric modeling of crystal morphology, and (2) computationally efficient simulation of macroscopic powder systems. Addressing this challenge is imperative for advancing density evolution prediction in PBX[26,27].

Based on the aforementioned research background, this paper establishes a two-dimensional mesoscale numerical model. The model utilizes Python programming to generate a large number of irregular polygonal crystal particles with random geometries, and incorporates thin coating layers surrounding the crystals to achieve accurate simulation of Polymer Bonded Explosive (PBX) particles. Through uniaxial compression numerical experiments, the mechanical response characteristics of PBX simulated explosives during the compaction process were systematically investigated, with particular focus on analyzing the stress distribution patterns, crystal damage evolution mechanisms, and temperature field variations under different friction coefficients.

Mechanical properties of crystals and Preparation of granular materials

Study on mechanical behavior of HMX and Na_2SO_4 crystals

Cyclotetramethylene tetranitramine (HMX), an organic compound[28,29], has the chemical formula $C_4H_8N_8O_8$. There are four crystalline forms of HMX, which are α-HMX, β-HMX, γ-HMX and δ-HMX. At present, the crude α-HMX is generally synthesized by acetic anhydride method at home and abroad, and then refined to obtain the pure product. Compared with other crystal forms, α-HMX is not stable under adverse conditions such as high temperature, high pressure and external stimulation, so it is necessary to carry out crystal transformation treatment to obtain a more stable crystal form. α-HMX crystals can be treated by waste acid crystallization, mixed solvent crystallization, nitric acid crystallization and other crystallization methods to obtain β-HMX crystals. β-HMX crystal is the most stable and practical at room temperature, which is widely used in military and industrial fields, especially in missile warhead charge, anti-tank charge and rocket propellantt, etc. γ-HMX, as an important crystal form of HMX, has unique physical and chemical properties. And its high density has the advantage of higher energy output in explosive formulations. It is difficult to obtain purer crystals because it is sub-stable at room temperature and requires high cooling rate during preparation.δ-HMX has a regular cavity structure, which is one of the main factors for the formation of hot spots and is sensitive to temperature and pressure.β-HMX crystals, with its excellent properties, have a wide range of applications in the fields of

chemistry, materials science, explosion mechanics and other fields. In fact, the crystals used in PBX explosives are all β-type[30] which is stable at room temperature. Due to the high danger of PBX in the actual process, Na_2SO_4, $Ba(NO_3)_2$, BaSO4, and white sugar crystals are generally selected for the study instead. Considering the toxicity and other influencing factors, Na_2SO_4 is finally selected for the study.

The mechanical properties of Na_2SO_4 and β-HMX crystals are tested by using the micromechanical loading experimental platform. To facilitate a direct comparison between the two materials, the experiment selected two similarly shaped, near-spherical particles with comparable dimensions: the β-HMX crystal has a diameter and height of 0.31 mm, while the Na_2SO_4 crystal measures 0.35 mm in both diameter and height. During the experiment, a constant and precise loading rate of 0.1 mm/min is adopted to ensure the accuracy and comparability of experimental data. The choice of this loading rate aims at applying external force slowly and uniformly, so that every tiny change of the crystal can be captured during the force application process. The stress-strain curve obtained from the test is shown in Fig. 1.

Through comparative analysis of the compressive mechanical behavior and load-displacement curves of the two crystals, the study revealed that both materials exhibit typical mechanical characteristics of brittle materials. The load-displacement curves clearly demonstrate two distinct phases: the elastic phase and the failure phase. During the initial elastic loading phase, both crystals undergo reversible elastic deformation under slow indenter compression. In this phase, no internal cracks are generated, and the crystals demonstrate excellent elastic recovery capability. The load-displacement curve in this region shows a linear relationship, with its slope representing the material's elastic modulus - a key parameter for evaluating a material's resistance to elastic deformation. Experimental measurements showed the elastic modulus of HMX crystal to be 2922.5 MPa, compared to 2092.4 MPa for Na_2SO_4 crystal, indicating that HMX possesses superior resistance to elastic deformation under identical stress conditions. When the load reaches a critical value, the crystals enter the failure phase where internal cracks initiate and propagate rapidly, leading to complete loss of load-bearing capacity. Notably, there exists a significant difference in their failure strengths: HMX crystal exhibits a failure load of 80.1 MPa, while Na_2SO_4 crystal only reaches 35.3 MPa. Despite these quantitative differences in mechanical parameters, both materials demonstrate highly similar mechanical response patterns and failure morphology characteristics throughout the loading process. Considering the potential hazards of HMX as a high explosive and the fact that Na_2SO_4 crystal not only offers higher safety but also exhibits mechanical behavior remarkably similar to HMX, the selection of Na_2SO_4 as a simulant material for HMX in compaction studies provides a safe and reliable approach to investigate the pressing process.

Preparation of granular materials

The commonly used methods for preparing explosive granules include mechanical grinding, direct method, solution-water suspension method, spray drying method and so on. Among them, the direct method and solution-water suspension method are the simplest and have good coating effect, which are often used to

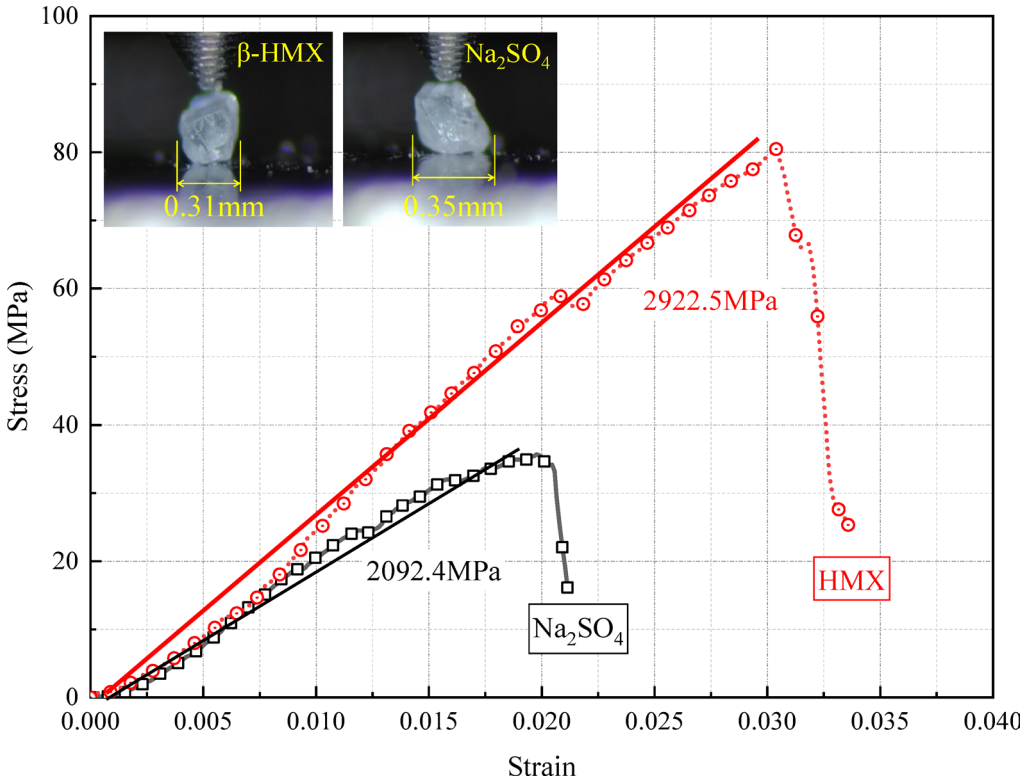

Fig. 1. Stress-Strain curve of crystal particles.

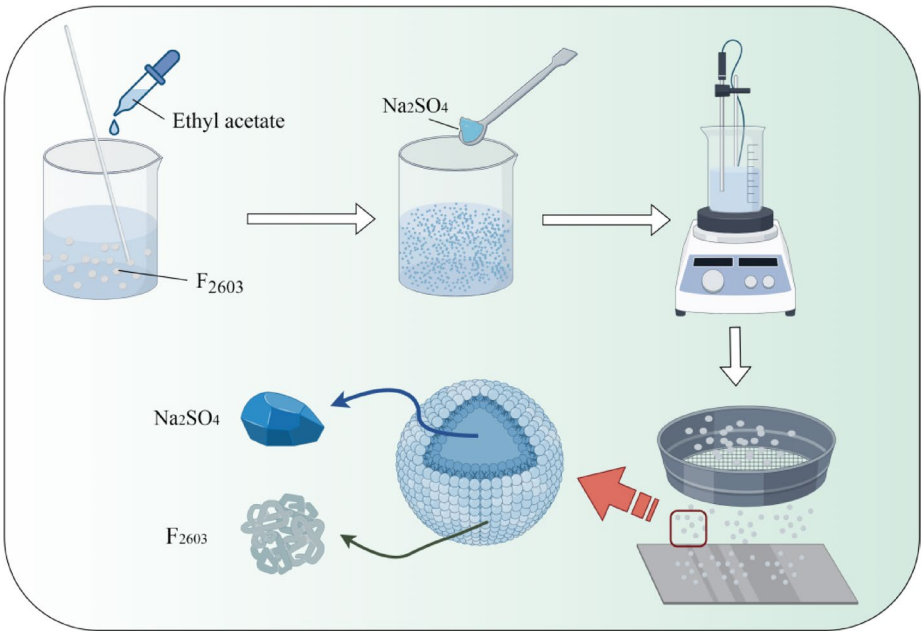

Fig. 2. Preparation process of granular materials.

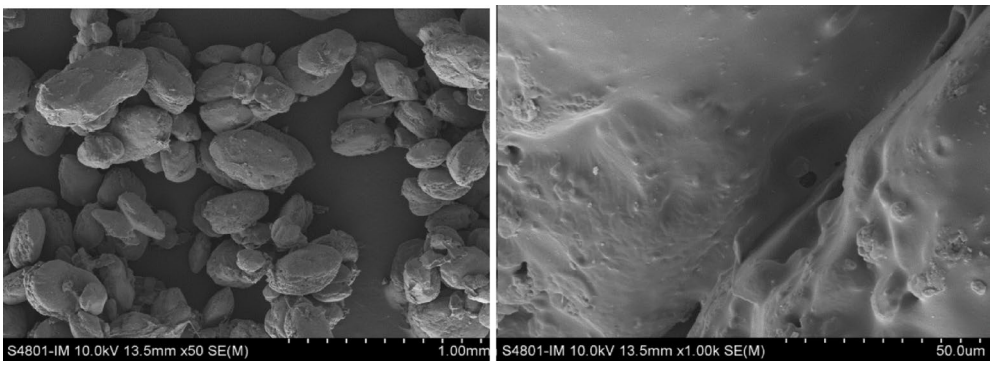

Fig. 3. The finished product of granular simulated explosive.

prepare granular in the laboratory. Because the simulated explosive uses Na_2SO_4 crystals, which are easily soluble in water, the direct method is chosen for the preparation of the granular simulated explosive. The preparation can be divided into several steps: dissolving, stirring, drying and sieving. During the preparation process, fluoroelastomer F2603 (5 wt%) was dissolved in ethyl acetate. The mixture was placed in a constant-temperature water bath and heated to 60 ± 2 °C with continuous stirring at 300 rpm for 2 h until complete dissolution. Subsequently, pre-dried Na_2SO_4 crystals (95 wt%) were gradually added to the solution, and stirring was continued at 200 rpm for 30 min to ensure uniform coating on the crystal surfaces. The mixture was then placed in a fume hood for natural solvent evaporation over 24 h. After the solvent had substantially evaporated, the material was transferred to a vacuum drying oven and dried for 6 h until a constant weight was achieved. Finally, the product was classified by sieving through No. 8 and No. 12 standard sieves, and particles between 1.7 mm and 2.36 mm were collected as experimental samples. The fabrication process is shown in Fig. 2.

The Na_2SO_4 crystals used in the experiment exhibited a particle size distribution with d_{50} of 300–320 μm. Figure 3 presents the microscopic morphology of the prepared granular material, showing that a complete fluororubber coating layer has formed on the crystal surfaces. Characterization results indicate the final granular particles demonstrate uniform size distribution, predominantly ranging from 2 to 4 mm. This particle size enlargement results from the co-encapsulation of multiple crystal particles during the dissolution-recrystallization process.

Granular compression molding test

The fabricated granular simulated explosive are subjected to compression molding test as shown in Fig. 4. This experiment utilized a displacement-controlled mode for the compression molding test, with the compaction loading rate set at 0.5 mm/min. This rate was selected based on the following considerations: first, a lower

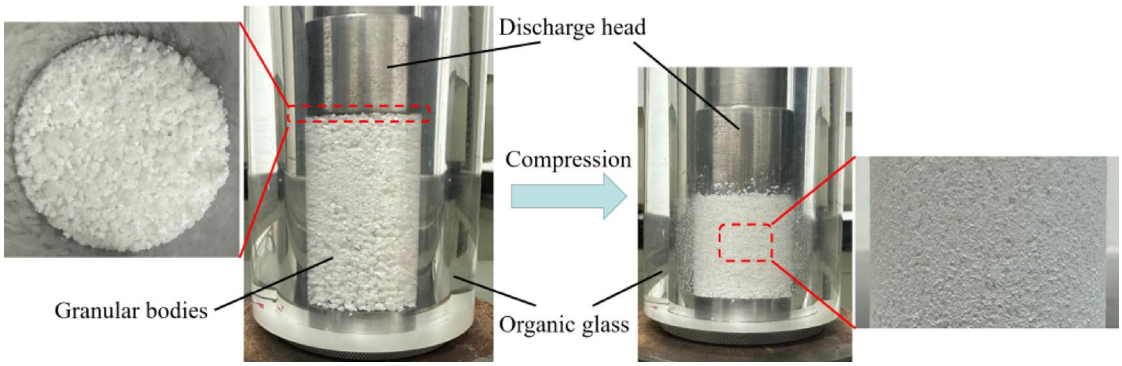

Fig. 4. Experiment on compression molding of granular simulators.

loading rate (under quasi-static conditions) effectively minimizes the influence of inertial effects and stress wave propagation on particle rearrangement behavior, ensuring the experimental process approximates a state of mechanical equilibrium; second, preliminary tests indicated that when the loading rate is below 1 mm/min, the stress-strain response of the granular material tends to stabilize more readily, facilitating observation of the gradual process by which the particles form a columnar structure. In order to observe the compacting process more clearly, the mold with high strength organic glass is used, and stainless steel is used for the discharge head and base. The granular simulated explosive is packed into a transparent mold, and the height of granular is about twice the inner diameter of the mold at the time of loading. At first, it is easy to see that the granular bodies are presented in granular form with a relatively loose structure and the boundaries between particles are clearly visible. When the discharge head is gradually compressed, the granular particles begin to squeeze each other, and eventually a tightly structured column grain is formed. However, by observing the molded column grain and mold, it can be found that the surface of the column grain is relatively rough, and a large number of polymer residues are tightly attached to the surface of the organic glass mold. This phenomenon is mainly attributed to the strong viscosity of polymer material itself, which makes it easy for polymer material to form close adhesion with the wall of mold when it is under pressure. This kind of rough adhesion is very unfavorable to the precision molding of column grain, so a small amount of graphite is generally added in the pressing process to improve this situation. This is because graphite has a strong lubricating effect, and a small amount of graphite will not have a greater impact on the mechanical properties of the explosive blast. The rough morphology of the surface of the formed column grain and the polymer residue on the surface of the mold indicate that the friction in the compacting process is an important influence that can not be ignored in the precision forming of granular materials.

Finite element simulation model

Geometric modeling

In performing geometric modeling, a model of granular crystals with specific structure is constructed. These particles are designed to have polygonal crystals inside and a layer of polymer material wrapped around the outside. The modeling process of the whole crystals is shown in Fig. 5. First, it is very important to define the initial boundary conditions, because it sets a clear range for the generation of particles. In this defined space, a series of circular particles with radius between 0.85 mm and 1.18 mm were randomly generated. In order to ensure that these particles do not overlap or cross each other in the physical space, a strict distance judgment mechanism is defined such that the particle is retained only if it will not cross other particles. Next, the upper limit of 2000 cycles is set. Once this cycle number is reached, the program will automatically stop running. For each successfully generated circular particle, we regard it as an effective model component. Subsequently, the radius of each circle is further adjusted and reduced by 0.1 mm as the radius of the circumscribed circle of the internal polygonal crystal. In the process of generating polygonal crystals, each crystal is randomly assigned 5–8 sides, and each angle of the polygon is calculated according to this number of sides to ensure that the polygon can perfectly adapt to its circumscribed circle. Finally, the internal polygons and external circular edges are retained, and a complete granular crystals model is formed.

As shown in Fig. 6, the two-dimensional assembly model can be divided into four parts: mold, discharge head, base and granular crystals. The internal width of the mold is 25 mm and the height is 50 mm. The discharge head and the base are located above and below the mold, respectively. The diameter of granular crystals follows the random distribution pattern of 8–12 meshes (that is, the diameter ranges from 1.7 mm to 2.36 mm), which ensures the diversity and randomness of the model in size. Each crystal consists of two parts, an inner polygon and an outer circle. The polygon represents the explosive crystal and the outer circle represents the polymer coating material, which has a thinnest area of 0.1 mm.

Constitutive model and material parameters

The Drucker-Prager (D-P) constitutive model is particularly suitable for simulating granular materials (e.g., soils, rocks, and powders) that exhibit hydrostatic pressure dependence and shear-induced densification characteristics. With its key parameters effectively characterizing pressure-sensitive yielding behavior and

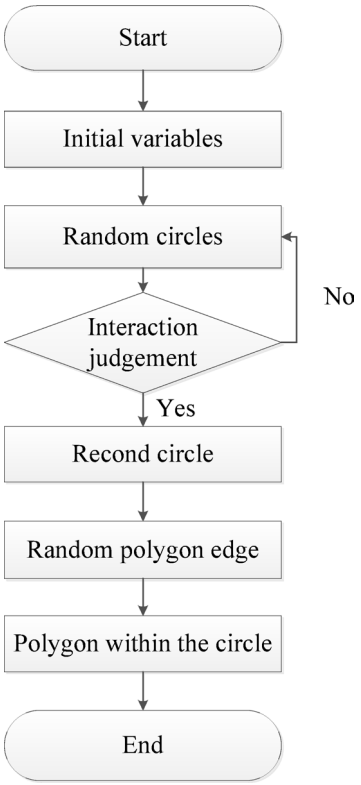

Fig. 5. Flow chart of granular modeling.

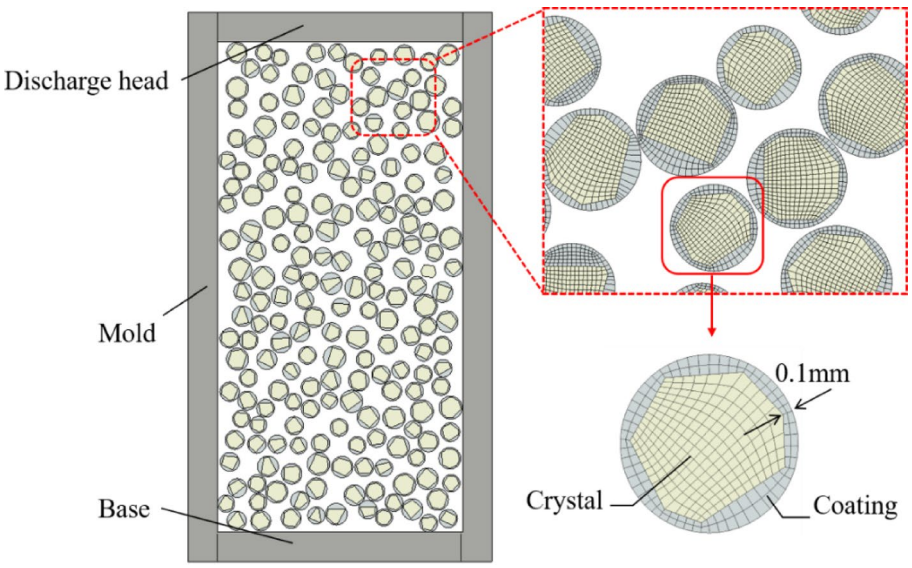

Fig. 6. Schematic diagram of two-dimensional model of granular materials.

volumetric plastic deformation, the D-P model demonstrates superior simulation performance under quasi-static loading and moderate confining pressure conditions. Therefore, this study adopts the D-P model to simulate the mechanical behavior of the outer coating material.

For crystalline materials with low fracture toughness and pronounced cleavage characteristics, the brittle cracking model proves more appropriate. It should be emphasized that the brittle cracking model must be coupled with a linear elastic material model, assuming the material strictly follows linear elastic behavior prior to crack initiation. Different from conventional fracture mechanics approaches, this model does not explicitly track "macroscopic" crack propagation paths. Instead, based on damage mechanics principles, it performs

independent constitutive calculations at each material point of the finite element model, characterizing the fracture process through the evolution of localized damage.

The crack initiation of brittle crack model is based on type I crack discrimination, but the post-cracking model contains both type I and type II cracks. The shear modulus after cracking decreases with the crack propagation, and the relationship between cracked and uncracked shear modulus is as follows:

$$G_c = \rho\left(e_{\mathrm{nn}}^{\mathrm{ck}}\right) G$$

Where, G is the shear modulus of the material without cracking; Shear retention factor$\rho\left(e_{\mathrm{nn}}^{\mathrm{ck}}\right)$ depends on crack propagation strain, and the correlation between them is as follows:

$$\rho\left(e_{\mathrm{nn}}^{\mathrm{ck}}\right) = \left(1\text{-}\frac{e_{\mathrm{nn}}^{\mathrm{ck}}}{e_{\max}^{\mathrm{ck}}}\right)^{p}$$

Where, p and$e_{\max}^{\mathrm{ck}}$ are material parameters.

Drucker Prager model is commonly used to simulate friction materials, and it can be used to describe materials whose compressive yield strength is greater than tensile yield strength, allowing long-term inelastic deformation of materials, which can simultaneously undergo inelastic expansion and inelastic shear. The expression of linear Drucker Prager criterion is as follows:

$$F = t - p\tan\beta - d = 0$$

$$t = \frac{1}{2}q\left[1 + \frac{1}{K} - \left(1 - \frac{1}{K}\right)\left(\frac{r}{q}\right)^{3}\right]$$

Where, β is the slope of linear yield on the p-t stress plane, which is commonly called the friction angle of the material; d is the cohesion of the material; K is the ratio of yield stress in triaxial tension to that in triaxial compression, which is used to control the correlation between the values of the intermediate principal stresses on the yield plane.

The hardening case is defined in uniaxial compression with a linear yield criterion incorporating a friction angle $\beta > 71.5°$($\tan\beta > 3$). When $K = 1$ and t = q, the yield surface is a Mises circle on the bias principal stress surface, in which case the yield stress is the same in triaxial tension and compression. In order to ensure that the yield surface remains convex, the value of K is $0.778 \le K \le 1.0$.

The relationship between cohesion d of materials and input data is as follows:

Hardening is defined by uniaxial compressive yield stress σ_c:

$$d = \left(1 - \frac{1}{3}\tan\beta\right)\sigma_c$$

Hardening is defined by uniaxial tensile yield stress σ_t:

$$d = \left(\frac{1}{K} - \frac{1}{3}\tan\beta\right)\sigma_t$$

Material parameters for polymeric materials were obtained through tensile tests and shear resistance tests, while the response characteristics of crystalline materials were acquired using a mechanical loading platform. During the experiments, crystal particles were placed between two indenters. Under a indenter displacement rate of 0.1 mm/min, the load-displacement curves of the crystals were recorded. Based on the morphological data of the crystals, the load-displacement curves were converted into stress-strain curves. The resulting material parameters are presented in Table 1.

Contact and friction coefficient

The compression behavior of granular systems involves complex contact interactions among three primary interfaces: crystal-polymer coating contacts, interparticle contacts, and particle-mold contacts. These inherently discontinuous nonlinear boundary problems exhibit contact surface detachment upon separation and constraint invalidation when interfaces part. Modern finite element implementations typically employ a general contact algorithm that provides comprehensive solutions through four key features: (1) highly customizable contact definitions, (2) simultaneous handling of multiple contact regions, (3) significant reduction of manual configuration requirements, and (4) enhanced computational efficiency. Critical to implementation is the proper specification of interfacial properties, which decompose orthogonally into normal contact conditions preventing

	E (MPa)	μ	Cracking stress (MPa)	Angle of fricrtion (°)	Flowstress ratio	Dilation angle (°)
Crystal	2848.2	0.2	48.4	–	–	–
Coating	200	0.49	–	5.169	1	5.169

Table 1. Parameters of crystal and polymer Materials.

material penetration while permitting only compressive forces, and tangential contact conditions governed by friction models that constrain relative motion. The complete contact interface configuration is illustrated in Fig. 7, demonstrating this sophisticated yet computationally efficient approach to modeling particulate system contacts.

According to the smoothness of the contact surface, it can be divided into two cases, namely, the without friction model and the friction model[31]. If the friction of the contact interface can be ignored in the analysis process, it can be considered that the tangential direction of the interface can slide freely, and the model expression is as follows:

$$ {}^{t}\boldsymbol{F}_{T}^{A}={}^{t}\boldsymbol{F}_{T}^{B}=\mathbf{0} $$

When the friction of contact interface must be considered, the friction model should be adopted. The model is expressed as follows:

$$ \left|{}^{t}\boldsymbol{F}_{T}^{A}\right|=\left[\left({}^{t}F_{1}^{A}\right)^{2}+\left({}^{t}F_{2}^{A}\right)^{2}\right]^{1/2}\leq\mu\left|{}^{t}\boldsymbol{F}_{N}^{A}\right| $$

Where, μ is the friction coefficient; $\left|{}^{t}\boldsymbol{F}_{T}^{A}\right|$ and tangential and normal contact force values respectively.

When the contact surface has no relative sliding, the expression is as follows:

$$ {}^{t}\bar{v}_{T}={}^{t}v_{T}^{A}-{}^{t}v_{T}^{B}=0 $$

At this point:

$$ \left|{}^{t}\boldsymbol{F}_{T}^{A}\right|<\mu_{s}\left|{}^{t}\boldsymbol{F}_{N}^{A}\right| $$

Where, ${}^{t}\bar{v}_{T}$ is the speed of the master node relative to the slave node; μ_s is the coefficient of static friction.

When the contact surface has relative sliding, the expression is as follows:

$$ {}^{t}\bar{v}_{T}={}^{t}v_{T}^{A}-{}^{t}v_{T}^{B}\neq 0 $$

At this point:

$$ \left|{}^{t}\boldsymbol{F}_{T}^{A}\right|=\mu_{d}\left|{}^{t}\boldsymbol{F}_{N}^{A}\right| $$

Where, μ_d is the dynamic friction coefficient, which is generally less than the static friction coefficient.

When granular materials are compressed, the contact surface will generate heat due to the occurrence of small sliding, resulting in an increase in the temperature of the particle surface. Friction heat generation is a transient heat conduction problem, and its virtual displacement principle is as follows:

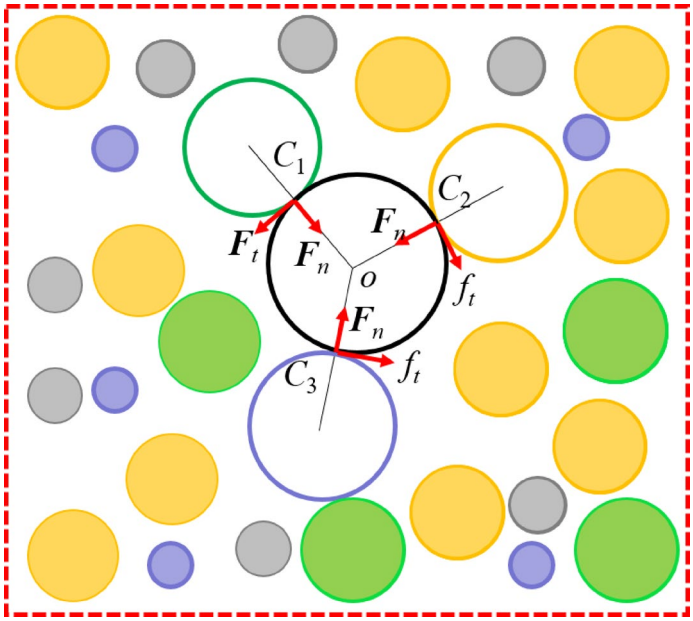

Fig. 7. Schematic diagram of contact interface.

	Thermal conductivity (w/K/m)	Specific heat (J/kg/K)
Crystal	0.462	978
Coating	0.25	1150

Table 2. Heat transfer coefficient.

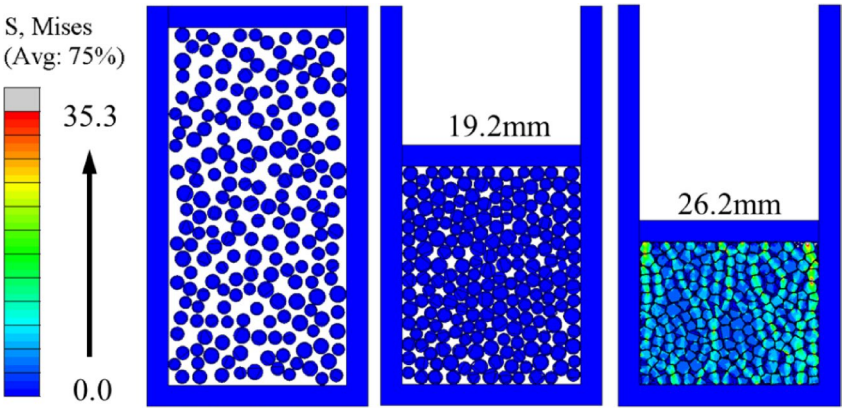

Fig. 8. Stress nephogram of particles compaction process.

$$\dot{T} = [N]\{\dot{q}\}$$

Among them,

$$\delta T = [N]\,\delta\{q\}$$
$$\nabla T = [B]\{q\}$$
$$\nabla(\delta T) = [B]\,\delta\{q\}$$

Substitute the interpolation formula into:

$$\{\delta q\}^T([K]\{q\} + [C]\{\dot{q}\} - \{Q\}) = 0$$

Among them,

$$[K] = \int_{\Omega} k[B]^T[B]\,d\Omega$$
$$[C] = \int_{\Omega} \rho C[N]^T[N]\,d\Omega$$
$$\{Q\} = \int_{\Omega} Q[N]^T\Omega + \int_{\Gamma_2} \bar{q}[\bar{N}]^T d\Gamma + \int_{\Gamma_3} hT_0[\bar{N}]^T d\Gamma$$

Where, $[K]$ is the heat conduction matrix; $[C]$ is the specific heat matrix; $\{Q\}$ is the equivalent node heat flow.

When carrying out simulation calculation, it is necessary to give the thermal conductivity and specific heat capacity of the material, and the heat transfer coefficient is shown in Table 2[18].

The results and analysis of compression molding

Compaction process

Figure 8 presents the stress nephogram illustrating the progressive compaction of granular materials during the compression molding process. The initial loose packing state exhibits scattered particle distribution with significant interparticle voids. As the discharge head advances, particle flow and rearrangement initiate in the direct loading region. At the critical displacement of 19.2 mm, substantial interparticle contact develops with gradually increasing interaction forces, while particle morphology remains largely intact - indicating the dominance of granular flow over plastic deformation at this stage. Further loading induces pronounced particle deformation, facilitating tighter packing and void filling by the polymer coating material, thereby enhancing overall compactness and structural integrity. Upon reaching 26.2 mm displacement, well-developed stress

chains become clearly visible, propagating vertically through the entire structure and demonstrating both the stress transmission pathways and the complex dynamic interactions within the particle assembly.

Two phases of compression process are shown in Fig. 9, which clearly reveals two key phases in the compression molding process: the particle flow stage and the particle extrusion deformation phase. In the particle flow phase, the granular particles start to flow due to the gradual compression effect of the discharge head. This phase is characterized by a significant reduction and filling of the voids, and the relative position of the particles is continuously adjusted to the external pressure. Because of the large voids between particles at this time, the discharge head can produce large displacement only by applying a relatively small load. This stage is the process of particle arrangement and initial densification, which lays the foundation for subsequent high-density alignment and close contact. When it is compressed to 38.4% of the height of the mold (that is 19.2 mm), the compacting process enters the stage of particle extrusion deformation. At this phase, because most of the internal voids have been compressed, the number of particles per unit volume has increased significantly. The contact area between particles increases, and the interaction force also enhanced. At this time, if compression is carried out again, the load to be required by the discharge head will rise sharply. This phase is the key period in which the interaction between particles plays a leading role, and it is also the most energy-consuming part in the process of compression molding. Combined with the stress change in the compacting process, it can be found that the main reason for the sharp increase of load is the mutual compression between crystals. As polygonal crystals are characterized by sharp corners, these corners often become the main areas of stress concentration during the compacting process. With the deepening of compacting process, the stress value at the corner of the crystal keeps rising until it reaches the yield strength or fracture strength of the material, thus causing the plastic deformation or fracture of the crystal.

Mechanical behavior of compression molding with different friction coefficients

In order to deeply investigate the specific effects of different friction coefficients on the mechanical behaviors during the compression molding process. In this study, four different values of friction coefficient are set, namely 0.0 (representing the ideal state of complete friction-free), 0.1, 0.2 and 0.3, which cover a wide range from extremely low friction to medium friction. It is worth noting that, except for the key variable of friction coefficient, all other model settings are consistent to ensure the accuracy and comparability of experimental results.

The load displacement curves under different friction coefficient conditions are shown in Fig. 10, which intuitively shows the influence of the friction coefficient on the mechanical behavior during the compression molding process. In particular, significant differences are presented in the two different phases of compression molding. In the first phase, that is, the particle flow stage, the effect of friction coefficient on this process is relatively small due to the relatively large void spacing between the particles and the limited mutual contact area between the particles. However, the situation changes significantly when the compacting process enters the second phase, that is, the particle extrusion deformation stage. With the gradual reduction of the void between particles and the extrusion deformation of polymer materials, the mutual contact between particles becomes closer and more frequent. At this time, the influence of the friction coefficient on the compacting process is

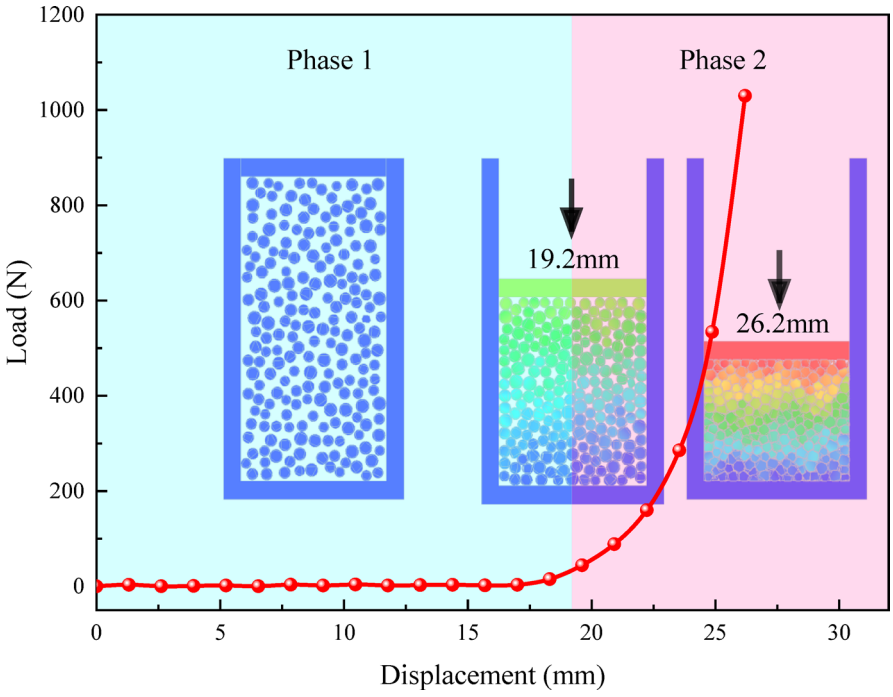

Fig. 9. Two phases of compression process.

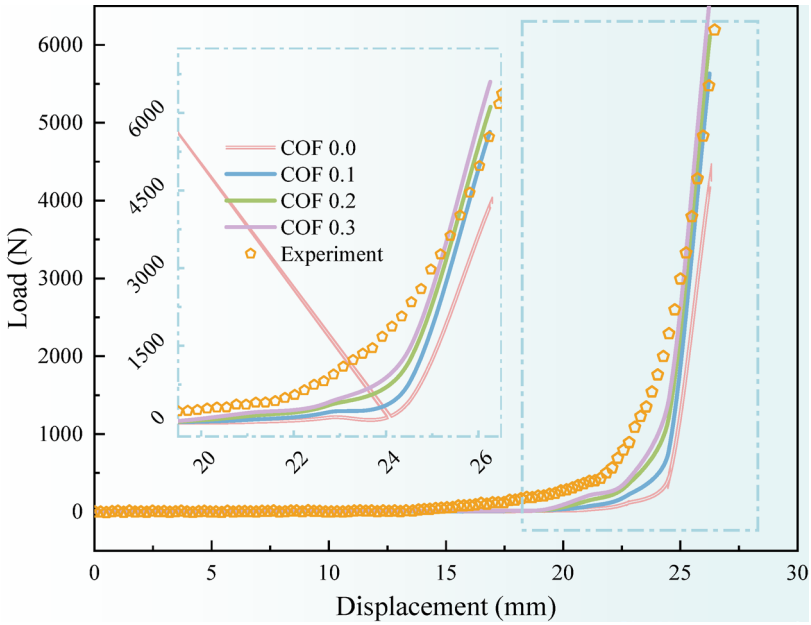

Fig. 10. Load-displacement curves with different friction coefficients.

significantly enhanced, which not only affects the sliding and rolling behaviors between the particles, but also directly relates to the overall stress distribution and compacting efficiency. Specifically, the increase of friction leads to an increase in the support reaction force during the compacting process. Under the same displacement condition, the greater the friction coefficient, the greater the compression reaction force required. For example, when the compression displacement reaches 26.2 mm, the supporting reaction force under the condition of no friction is 4253.2 N, while the supporting reaction force is as high as 6599.8 N when the friction coefficient is 0.3, with a difference of 31.6%. This result clearly demonstrates the importance of the friction coefficient in the second stage of compression molding. It is worth noting that with the further increase of friction coefficient, the increase of supporting reaction force shows a decreasing trend. This means that when the friction coefficient reaches a certain critical value, its contribution to the support reaction force of compression molding will gradually weaken.

Comparison of the experimental and simulation, it is found that there are some differences between them at the initial moment of the second phase of molding. Specifically, the experimental test data show an inflection at this moment earlier than the simulation data, that is, the compacting process in the experiment enters the stage of particle extrusion deformation earlier. This difference is mainly attributed to the simplified treatment of polymer coating by the simulation model. In fact, the polymer materials in granular materials are loose and gradually change from loose state to dense state when subjected to compressive load. However, in simulation modeling, it is usually assumed that the polymer material is already in a compacted state in order to simplify calculations and improve efficiency. Although this simplified treatment can reflect the basic law of compression molding to a certain extent, it may deviate from the actual situation in some details, which leads to the difference between experimental and simulation data.

Figure 11 presents a comparative analysis of crystal damage evolution under varying friction coefficients while maintaining identical compacting conditions. The results demonstrate a pronounced positive correlation between the friction coefficient and crystal damage propagation. In the frictionless condition ($\mu = 0$), the damage rate remains minimal at 0.9%, suggesting relatively benign inter-crystalline interactions. However, systematic increases in friction coefficient induce progressive damage escalation: $\mu = 0.1$ corresponds to 4.6% damage, $\mu = 0.2$ yields 10.3%, and $\mu = 0.3$ produces significant damage reaching 14.5%. This quantitative progression unequivocally establishes friction coefficient as a critical determinant of crystal integrity. Spatial analysis reveals distinct damage distribution patterns corresponding to friction intensity. At $\mu = 0.1$, damage predominantly localizes at grain boundaries due to combined effects of external compressive stresses and intergranular friction. The transition to $\mu = 0.3$ induces a dual damage mechanism: (1) intensified boundary degradation and (2) emergent intra-granular damage resulting from enhanced crystalline lattice stresses. This transition demonstrates how elevated friction coefficients fundamentally alter damage kinetics by promoting stress penetration from grain boundaries into crystalline matrices, thereby establishing a comprehensive damage network throughout the material microstructure.

Analysis of temperature change of compacting forming

Because of its unique physical and chemical characteristics, granular explosives have the risk of explosion accidents caused by hot spots in the process of compression molding. In order to deeply investigate the causes of hot spots, the temperature distribution of compression molding is simulated and analyzed. Since the temperature change in the compacting process is closely related to the friction coefficient, and the friction in the actual

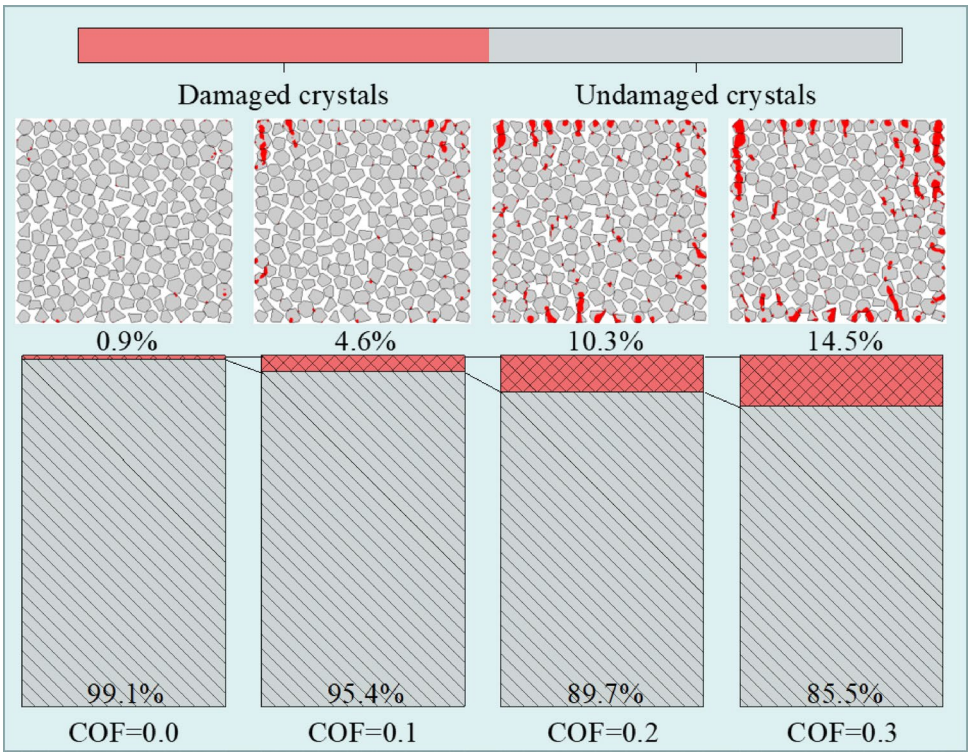

Fig. 11. Crystal damage diagram under different friction coefficients.

situation is more complicated, this study analyzes the friction coefficient of 0.3 as an example, aiming to get the temperature distribution in the most dangerous situation. The change of crystal temperature can intuitively reflect the generation mechanism of hot spots, and the extraction temperature distribution is shown in Fig. 12. It can be clearly seen from the figure that the temperature of the crystal reaches a maximum of 52.7℃, which is an increase of 32.7℃compared with the initial temperature. Although this temperature change has not yet reached the critical point of triggering an explosive explosion, the simulation results can provide us with some valuable clues. Combined with the crystal damage diagram for comprehensive analysis, the specific location of the temperature change can be observed more intuitively. It is not difficult to find that the temperature change mainly occurs in the angular part of the crystal, especially at the parts in contact with the side walls, and the temperature change is particularly obvious. This phenomenon suggests that the generation of hot spots is closely related to the friction between the mold walls and the crystals, as well as the possible breakage of the crystals during the pressing process. When the crystal is crushed by pressure, the chemical bonds inside it can break and release energy, which lead to the increase of local temperature.

To quantify the impact of the friction coefficient on hotspot formation, a simulation system was used to compare the temperature response under four conditions: $\mu = 0$, 0.1, 0.2, and 0.3. The results show that the maximum temperature increases were 2.26 °C, 8.2 °C, 12.7 °C, and 32.7 °C, respectively, indicating a nonlinear positive correlation between the friction coefficient and temperature rise. Further analysis of the temperature distribution revealed that when $\mu = 0.1$, high-temperature points only sporadically appeared in the mold contact area; when $\mu \geq 0.2$, high-temperature regions significantly expanded to crystal-crystal contact interfaces and internal crystal cracks; when $\mu = 0.3$, the local maximum temperature reached 52.7 °C, and the high-temperature areas highly coincided with crystal damage locations. This suggests that high friction conditions not only intensify frictional heating at interfaces but also indirectly trigger the release of chemical bond fracture energy by promoting crystal fracture, forming a vicious cycle of thermo-mechanical coupling. The analysis results for different friction coefficients show that when the friction coefficient is 0, the maximum temperature rise is 2.26 °C. Under this condition, the influence of friction is eliminated, and the temperature increase is solely due to crystal fracture. This further indicates that crystal breakage during the molding process leads to a temperature rise.

Based on the above analysis, we can think that the main reason for the hot spot is the friction between the mold wall and the crystal as well as the fracture of the chemical bond when the crystal is broken. In order to effectively avoid the generation of hot spots and reduce the risk of explosion accidents, a series of targeted measures need to be taken. Among them, reducing the roughness of the mold is an effective method, which can reduce the friction between the mold wall and the crystals, thus reducing the magnitude of the temperature increase. In order to effectively avoid hot spots and reduce the risk of explosion accidents, a series of targeted measures need to be taken. Among them, reducing the roughness of the mold is an effective method, which can reduce the friction between the mold wall and the crystal, thus reducing the amplitude of temperature rise. In addition, it is also very important to improve the fit of the discharge head to the mold, which can ensure that the

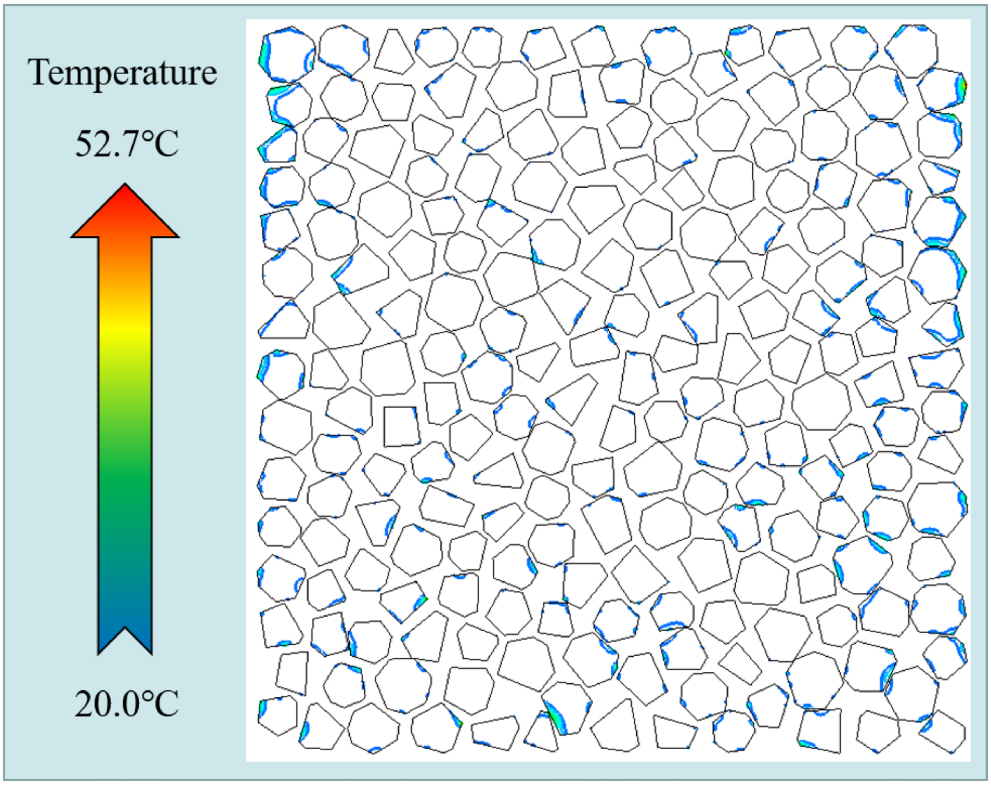

Fig. 12. Temperature distribution of compression molded crystals.

compacting process runs smoothly and reduces the additional friction and shear caused by improper matching. Accordingly, a synergistic optimization approach can be implemented from three aspects: mold interface optimization (e.g., applying low-friction coatings), intelligent regulation of process parameters (e.g., establishing digital control), and pretreatment of crystal materials (e.g., reducing direct crystal contact), so as to enhance the safety of the molding process.

Conclusion

The mechanical behavior of the compression molding of granular simulated explosives is analyzed by using experiments and two-dimensional mesoscopic model, and the influence law of friction coefficient on the support reaction force and crystal breakage is obtained. The hot spot generation mechanism is obtained by analyzing the temperature response of the compression molded crystals. The main conclusions are as follows:

(1) The compaction process of granular materials can be roughly divided into two phases, respectively, the particle flow phase and the particle extrusion deformation phase. The particle flow phase is mainly characterized by the filling of pores, and a small compressive load can lead to a large displacement at this phase. The mechanical behavior of particle extrusion deformation stage is transformed into the mutual extrusion force between polymer material filling pores and crystals, and a small displacement at this stage can lead to a sharp increase in the load;

(2) The simulation and experimental results indicate that the friction behavior in the compaction process of granular materials can not be ignored, and the friction coefficient leads to changes reaction force and the degree of crystal damage in the compression molding. The model reaction force with a friction coefficient of 0.3 is 35.5% higher than that in the case of no friction, and the crystal damage rate increases by 13.6% when the friction coefficient is increased from 0 to 0.3.

(3) Compared with the initial temperature, the temperature of the compressed crystal is increased by 32.7℃, which is not so high as to make the explosives explode. However, the temperature distribution results show that the hot spots are caused by the friction between the mold wall as well as the breakage of chemical bond is broken when the crystal is broken. The hot spot generation can be suppressed by reducing the roughness of the mold, improving the fit between the discharge head and the mold, and reducing the friction between the granular explosive and the mold.

Data availability

The authors may provide data upon reasonable request. If any researchers want to get the data from this study, please contact Xiaoyang Wu. Email: wxyxian204@163.com.

Received: 31 March 2025; Accepted: 29 September 2025
Published online: 08 January 2026

References

1. Keyhani, A. et al. Energy dissipation in polymer-bonded explosives with various levels of constituent plasticity and internal friction. *Computational Materials Sci.*, (2018).
2. Leversee, R. A. et al. High-pressure isothermal equation of state of composite materials: A case study of LX-17 polymer bonded explosive[J]. *Appl. Phys. Lett.*, 2019,115(5).
3. Gong, Z. et al. The aging performance of acrolein pentaerythritol Resins-based casting PBX[J]. *Hanneng Cailiao = Chin. J. Energetic Mater.* **30** (6), 584 (2022).
4. Sevinc, A. & Edis, B. Effects of Slit plate design on mechanical properties of castable plastic bonded explosives[J]. *Propellants, Explos., Pyrotech.*, **49**(6): (2024).
5. Cao, S. et al. Design and performance of a low vulnerability PBX with HMX and Al[J]. *Hanneng Cailiao = Chin. J. Energetic Mater.*, (7):650. (2021).
6. Nie, P. et al. Study on the effect of NTO on the performance of HMX-Based aluminized Cast-PBX[J]. *Materials* **15** (14), 4808 (2022).
7. Voelkel, S. J. et al. Effect of lot microstructure variations on detonation performance of the triaminotrinitrobenzene (TATB)-Based insensitive high explosive PBX 9502[J]. *Combust. Flame*. **246**, 112373 (2022).
8. Bishop, R. L. et al. Safe operating temperatures for pressurized alkaline hydrolysis of HMX-Based Explosives[J]. *Ind. Eng. Chem. Res.* **39** (5), 1215–1220 (2000).
9. Guan, L. et al. Engineering design of Large-Scale cured PBX[J]. *Bing gong. Zi Dong Hua*. **29** (4), 23–24 (2010).
10. Woodrum, R. B. et al. Developing safe lathing parameters for PBX 9501[J]. *Propellants, Explos., Pyrotech.* **43** (8), 779–788 (2018).
11. Thompson, D. G., Deluca, R. & Brown, G. W. Time-Temperature Analysis, tension and compression in PBXs[J]. *J. Energ. Mater.* **30** (4), 299–323 (2012).
12. Herman, M. J. et al. Composite binder, processing, and particle size effects on mechanical properties of non-hazardous high explosive surrogates[J]. *Powder Technol.* **391**, 442–449 (2021).
13. Jia, D. et al. Power function Mohr-Coulomb strength criterion and failure characteristics of PBX simulant under Compression-Shear stress State[J]. *Hanneng Cailiao = Chin. J. Energetic Mater.*, **2020**(1):32 .
14. Chen, L. et al. Compressive behavior and damage evaluation of a PBX substitute material[J]. *Mech. Adv. Mater. Struct.* **24** (9), 737–744 (2017).
15. Tan, H. et al. The Mori–Tanaka method for composite materials with nonlinear interface debonding[J]. *Int. J. Plast.* **21** (10), 1890–1918 (2005).
16. Zhang, M. et al. Study on compression-expansion behaviour of PBXs substitutive materials[J]. *Plast. Rubber Compos.* **48** (4), 137–148 (2019).
17. Hagengruber, T. et al. Multiscale numerical investigation of ratchet growth damage effects in PBX 9502[J]. Propellants, explosives, pyrotechnics, 2023,48(11).
18. Tang, H. et al. Two dimensional numerical simulation for mesoscopic mechanics behaviors of PBX in pressing Processes[J]. *Hanneng Cailiao (Chinese J. Energetic Materials)*, 2016,24(7).
19. Sun, H. et al. Research progresses and prospects of compression molding of High-performance PBX[J]. *Zhongguo Jixie Gongcheng = China Mech. Eng.* **35** (1), 160 (2024).
20. Sun, H. et al. Mechanism of uneven densification in PBX compression molding[J]. *Int. J. Mech. Sci.* (2024).
21. Xiao, Y. et al. Multiscale modeling for dynamic compressive behavior of polymer bonded explosives[J]. *Int. J. Mech. Sci.* **242**, 108007 (2023).
22. Guo, Y. et al. Mechanical behavior of PBX with different HMX crystal size during die pressing: experimental study and DEM simulation[J]. *Compos. Sci. Technol.* **222**, 109378 (2022).
23. Pan, Q. et al. Meso-Simulation and experimental research on the mechanical behavior of an energetic Explosive[J]. *Coat. (Basel)*, 11(1):64. (2021).
24. Xiaoshan, Z. et al. Damage behavior of high particle volume fraction composites with initial damage by finite element meso-modeling[J]. *Composite Struct.*, (2024).
25. J C, N. K L, A. J, T. B. Exploring pressure-dependent inelastic deformation and failure in bonded granular composites: an energetic materials perspective[J]. *Mech. Mater.*, (2023).
26. Wang, X., Wu, Y. & ,Huang, F. Numerical mesoscopic investigations of dynamic damage and failure mechanisms of polymer bonded explosives[J]. *Int. J. Solids Struct.*, 12928–12939. (2017).
27. Youcai, X. et al. Multiscale modeling for dynamic compressive behavior of polymer bonded explosives[J]. *Inter. J. Mech. Sci.*, (2023).
28. Gallagher, H. G., Sherwood, J. N. & Vrcelj, R. M. The growth and perfection of β-cyclotetramethylene-tetranitramine (HMX) studied by laboratory and synchrotron X-ray topography[J]. *J. Cryst. Growth.* **475**, 192–201 (2017).
29. Shi, J. et al. Effects of binders on the phase transition behavior of HMX[J]. *Hanneng Cailiao = Chin. J. Energetic Mater.* **30** (6), 550 (2022).
30. Li, Y. et al. Mechanical,Thermal conductive properties and tablet impact sensitivity of Micro-nano-HMX based PBX[J]. *Hanneng Cailiao = Chin. J. Energetic Mater.*, (4):334. (2018).
31. Yuan, J. et al. An adaptive component mode synthesis method for dynamic analysis of jointed structure with contact friction interfaces[J]. *Comput. Struct.* **229**, 106177 (2020).

Author contributions

Xiaoyang Wu (Corresponding Author): Conceptualization, Methodology, Software, Investigation, Formal Analysis, Writing - Original Draft; Jun Tao (Corresponding Author) : Data Curation, Writing - Original Draft; Bo Wang: Experiment; Haichao Ren : Visualization, Investigation; YipingWang: Resources, Supervision;

Declarations

Competing interests

The authors declare no competing interests.

Additional information

Correspondence and requests for materials should be addressed to X.W. or J.T.

Reprints and permissions information is available at www.nature.com/reprints.